Atmospheric Environment 253 (2021) 118387

Contents lists available at ScienceDirect

Atmospheric Environment

journal homepage: http://www.elsevier.com/locate/atmosenv

# Importance of $NO_3$ radical in particulate nitrate formation in a southeast Chinese urban city: New constraints by $\delta^{15}N$-$\delta^{18}O$ space of $NO_3^-$

Zhongyi Zhang [a,b], Lin Cao [a,b], Yue Liang [a,b], Wei Guo [a,b], Hui Guan [c], Nengjian Zheng [a,b,*]

[a] Jiangxi Province Key Laboratory of the Causes and Control of Atmospheric Pollution, East China University of Technology, Nanchang, 330013, China
[b] School of Water Resources and Environmental Engineering, East China University of Technology, Nanchang, 330013, China
[c] The State Key Laboratory of Environmental Geochemistry, Institute of Geochemistry, Chinese Academy of Sciences, Guiyang, 550081, China

## HIGHLIGHTS

- The $\delta^{15}N$–$NO_3^-$ and $\delta^{18}O$–$NO_3^-$ ranged from −1.9‰ to +12.1‰ and +69.1‰ to +95.5‰, respectively.
- The daily $\delta^{15}N$–$NO_3^-$ was independent with the corresponding $\delta^{18}O$–$NO_3^-$ ($R^2$ = 0.06, $p > 0.05$).
- Results highlighted the importance of $NO_3$ radical in NO*x* oxidation in polluted urban environment.

## GRAPHICAL ABSTRACT

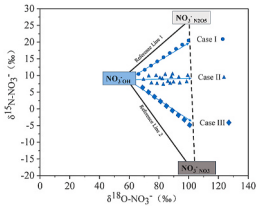


## ARTICLE INFO

*Keywords:*
Nitrate
$NO_3$ radical
$\delta^{15}N$-$\delta^{18}O$ space
$PM_{2.5}$
Nanchang

## ABSTRACT

Stable nitrogen and oxygen isotopic signatures of nitrate in atmospheric fine-mode particulate (as $\delta^{15}N$–$NO_3^-$ and $\delta^{18}O$–$NO_3^-$ in $PM_{2.5}$) was proposed to be useful in distinguishing the sources and oxidation chemistry of NO*x* (NO*x* = NO + $NO_2$). In the present study, the chemical oxidation processes of atmospheric NO*x* in urban Nanchang, the capital of Jiangxi province, southeast of China were estimated based on the $\delta^{15}N$-$\delta^{18}O$ space of $NO_3^-$. Daily $PM_{2.5}$ samples (n = 91) were collected during wintertime of 2017–2018 (1 November to 31 January), the major water-soluble inorganic ions and the dual isotopic signatures of $NO_3^-$ were measured. During the observations, the $NO_3^-$ concentrations in $PM_{2.5}$ varied widely from 0.8 μg/m$^3$ to 57.7 μg/m$^3$, on average of 15.5 ± 6.7 μg/m$^3$. The $\delta^{15}N$–$NO_3^-$ and $\delta^{18}O$–$NO_3^-$ also ranged widely, from −1.9‰ to +12.1‰ (+6.5 ± 3.7‰) and +69.1‰ to +95.5‰ (+85.9 ± 17.7‰), respectively. The daily $\delta^{15}N$–$NO_3^-$ was observed to be independent with the corresponding $\delta^{18}O$–$NO_3^-$ ($R^2 = 0.06$, $p > 0.05$), which contrasted with many previous reports. By linking the $\delta^{15}N$–$NO_3^-$ to the NO*x* oxidation chemistry, we tried to explore the environmental significance of the $\delta^{15}N$-$\delta^{18}O$ space of $NO_3^-$. Our results suggested that the nocturnal pathways (e.g., $N_2O_5$ hydrolysis and $NO_3$ radical reacted with hydrocarbons: $NO_3$+HCs) dominated the chemical conversion of NO*x* to $NO_3^-$ in the wintertime of Nanchang, with an average fractional contribution of 60%. Interestingly, results also indicated the importance of the $NO_3$+HCs channel in NO*x* oxidation (on average of 33%), which can reach 45% during extreme nitrate aerosol polluted days. Our observations highlighted the importance of $NO_3$ radical in NOx oxidation and particulate nitrate formation in polluted urban environment.

* Corresponding author. Jiangxi Province Key Laboratory of the Causes and Control of Atmospheric Pollution, East China University of Technology, Nanchang, 330013, China.
*E-mail address:* zhengnengjian@ecut.edu.cn (N. Zheng).

https://doi.org/10.1016/j.atmosenv.2021.118387
Received 29 September 2020; Received in revised form 21 January 2021; Accepted 30 March 2021
Available online 2 April 2021

## 1. Introduction

Anthropogenic emission of nitrogen oxides (NO*x*, e.g., NO, $NO_2$) has significantly altered the natural nitrogen cycle and linked to numerous serious environmental and health problems (An et al., 2019; Fang et al., 2011b; Geng et al., 2019). Global investigations pointed out that fossil-fuel combustion and agricultural activity were responsible for the NO*x* emission to the atmosphere (Fang et al., 2015; Geng et al., 2014; Vasilakos et al., 2018; Song et al., 2021). Once emitted to the atmosphere, the majority of NO*x* was oxidized into inorganic or organic nitrate, which was the dominant sink for global NO*x* (Alexander et al., 2019; Womack et al., 2019). As depicted in Fig. 1, the NO*x* converted into inorganic nitrate mainly through three pathways in inland cities, which included: i) $NO_2$ oxidation by OH radicals in the daytime (termed as $NO_2$+OH); ii) hydrolysis of dinitrogen pentoxide ($N_2O_5$) on the surface of wet aerosols; iii) nitrate radicals ($NO_3$) reacting with saturated organic hydrocarbon (HC) compounds (as $NO_3$+HC; Seinfeld and Pandis, 2016). Generally, the channel of $NO_2$+OH dominated during the daytime and summer season, while the $N_2O_5$ hydrolysis and $NO_3$+HC channels were typically prevalent during winter and at night since the $N_2O_5$ and $NO_3$ radical were thermally unstable and easily photolyzed (Chang et al., 2019a; He et al., 2018).

The oxygen isotopic composition of nitrate in fine-mode particulate ($PM_{2.5}$), e.g., $\delta^{18}O$–$NO_3^-$ and $\Delta^{17}O$–$NO_3^-$ were suggested useful in inferring the relative importance of different channels of $NO_3^-$ oxidation pathways (Alexander et al., 2009; Hastings, 2004; Hastings et al., 2003; He et al., 2020; Michalski, 2005; Michalski et al., 2003; Savarino et al., 2016; Walters and Michalski, 2016; Wang et al., 2019; Fan et al., 2020). Usually, $NO_3^-$ produced via nocturnal channels of $N_2O_5$ hydrolysis and $NO_3$+HC were characterized by $^{18}O$-enriched signatures (e.g., 97‰ ~109‰), as the $N_2O_5$ and $NO_3$ radical can reach equilibrium with the oxidant of $O_3$ ($\delta^{18}O$–$O_3$ was predicted to be +117 ± 5‰ relative to international standard) during the chemical oxidation reactions (Fig. 2; Chang et al., 2019a; Fang et al., 2011a; He et al., 2020; Zong et al., 2020; Fan et al., 2020). In contrast, $NO_3^-$ generated through the $NO_2$+OH channel was registered as relatively lower $\delta^{18}O$ values. For example,

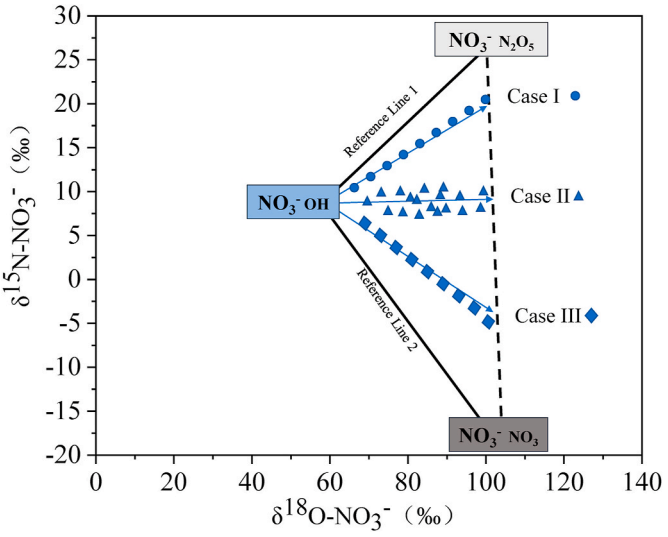


**Fig. 2.** Theoretical $\delta^{18}O$–$\delta^{15}N$ space of particulate nitrate generate through daytime channel (assuming $f_{NO2}$ = 0.8) and nighttime channels under the typical wintertime conditions of urban Nanchang. $\delta^{15}N$–$NO_2$ was assumed to be 0. The reference line 1 and 2 represented that nocturnal $NO_3^-$ formed completely through $N_2O_5$ and NO3+HC channels, respectively. In the real environment, $\delta^{18}O$ of nitrate may correlated with the corresponding $\delta^{15}N$ values positively (case I) or negatively (case III) or not (case II).

Fang et al. (2011a) suggested the endmember value of $\delta^{18}O$–$NO_3^-$ via $NO_2$+OH channel was approximately +55‰, which was mainly attributed to the involvement of significantly $^{18}O$-depleted OH during $NO_2$ transformation (Fang et al., 2011a). Therefore, the $\delta^{18}O$–$NO_3^-$ was extensively used to distinguish the relative contribution of daytime and nocturnal channels; however, it is difficult to differentiate the relative importance between $N_2O_5$ hydrolysis and $NO_3$+HC channels based only on the $\delta^{18}O$–$NO_3^-$ approach.

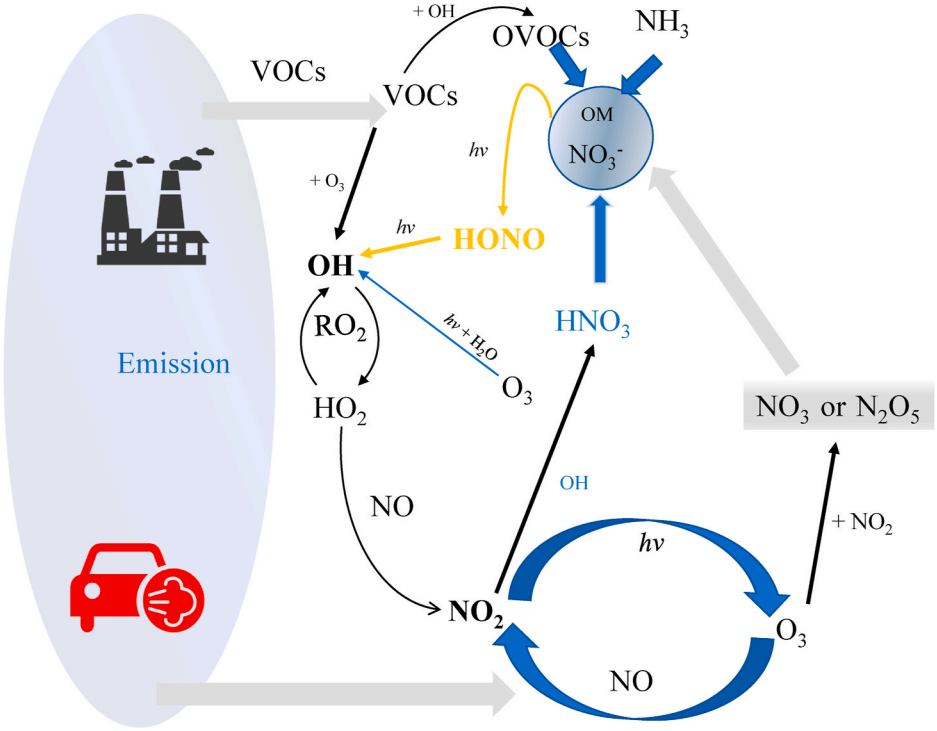


**Fig. 1.** Simplified schematic of the relevant particulate nitrate formation channels in polluted urban atmosphere (Lu et al., 2019). Bule marked chemical species dominant in daytime reaction, grey in nocturnal chemistry and the HONO triggered reactions are in debates.

While $\delta^{15}N–NO_3^-$ has been widely used to fingerprint the NO*x* sources (Hastings, 2004; Morin et al., 2008; Song et al., 2019; Walters et al., 2015c), previous theoretical researches suggested it may also provide valuable insights into the NO*x* oxidation chemistry at a process level (Walters and Michalski, 2015b, 2016). This was because the different oxidation mechanisms responsible for the formation of aerosol $NO_3^-$ may lead to distinctive nitrogen isotopic signatures that can be recorded in the environment media (e.g., $PM_{2.5}$, dry/wet deposition). As shown in Fig. 2, $NO_3^-$ generated through $NO_2$+OH pathway was registered as middle-ranking $\delta^{15}N$ values but most $^{18}O$-depleted signatures, while that through the $NO_3$+HC or $N_2O_5$ hydrolysis pathways was characterized by similar $^{18}O$-enriched signatures; however, the $NO_3$+HC channel was associated with $^{15}N$-depleted signatures, as contrasted to the $N_2O_5$ hydrolysis pathway which was significantly $^{15}N$-enriched (Walters and Michalski, 2016; Song et al., 2020; Liu et al., 2020; Zong et al., 2017). Therefore, the $\delta^{15}N$-$\delta^{18}O$ space of $NO_3^-$ may help to elucidate the fractional contribution of the three pathways in NO*x* oxidation processes. However, the imprinted signals of $\delta^{15}N–NO_3^-$ during the oxidation pathways can be impacted substantially by the changes in the emission sources of NO*x* and the underlying N fractionation effects. Taking the urban environment as an example, the dominant anthropogenic sources of NO*x* from fossil fuel combustion were characterized by relatively $^{15}N$-enriched values, while NO*x* emitted through nitrification and denitrification processes was usually $^{15}N$-depleted (Felix and Elliott, 2014; Felix et al., 2012; Walters et al., 2015a; Walters and Michalski., 2015b; Yu and Elliott, 2017). In brief, the environmental $\delta^{15}N–NO_3$ signatures were a hybrid of NO*x* source information and oxidation processes-mediated fractionation effect (Zong et al., 2017; Fan et al., 2020; Liu et al., 2020). This may be the reason that hindered the deep understanding of the environmental significance of $\delta^{15}N$-$\delta^{18}O$ space of $NO_3^-$ in NO*x* oxidation chemistry.

In the present study, the daily $PM_{2.5}$ samples (23.5h) were collected from 1 November 2017 to 31 January 2018 (n = 91) at the urban city of Nanchang, the capital of Jiangxi, located in the southeast of China (Fig. S1). The urban city of Nanchang still experienced severe haze pollution in recent years, in which the particulate nitrate was suggested as the predominant inorganic component in $PM_{2.5}$ (Xiao et al., 2020). The aerosol inorganic chemical species and properties (e.g., aerosol acidity), as well as the dual isotopic composition of nitrate were quantified, and those data were used to investigate the oxidation processes and factors that controlled the wintertime particulate nitrate formation in urban Nanchang. Our results highlighted the relative importance of nocturnal $NO_3$ radical chemistry, particularly the reaction of $NO_3$ radical with organic compounds in wintertime nitrate pollution in the urban environment.

## 2. Material and method

### 2.1. Site description and sampling

The sampling campaign was conducted on the Qingshanhu campus of Nanchang University (28°41′N, 115°56′E, Fig. S1) from 1 November 2017 to 31 January 2018. The campus is located in the old urban area of Nanchang city, about 3 km away from the Nanchang railway station and near the first-ring viaduct and Metro line No.1. The site is registered as a typical urban area for business and residents, with no industry and other point sources (Xiao et al., 2020). A total of 91 samples (89 p.m.$_{2.5}$ samples and 2 blank samples) were collected in the sampling campaign. The instruments were set on the roof of a six-story teaching building, approximately 25m above the ground. During the sampling campaign, the prevailing wind direction was northeast, with an average speed of 1.7 ± 0.7 m/s.

The $PM_{2.5}$ sampling procedure has been well-described elsewhere (Xiao et al., 2020; Zhang et al., 2020c). In brief, quartz fiber filters were pre-combusted at 450 °C for 3h to remove impurity then used for $PM_{2.5}$ collection with a high-volume air sampler (KC-1000, equipped with a $PM_{2.5}$ impactor). The duration of the daily sample was 23.5h at a flow rate of 1.05 $m^3$/h. $PM_{2.5}$ samples were immediately delivered to the laboratory and stored in the refrigerator once collected. Gaseous $HNO_3$ and particulate nitrate may be sampled simultaneously during the campaign, and therefore described as atmospheric inorganic nitrate in this study. The meteorological and air quality parameters (e.g., temperature, wind speed, and direction, relative humidity, hourly-resolution of NO, $NO_2$, $SO_2$, $O_3$) were acquired from the nearby station of Jiangxi Provincial Center for Environment Monitoring (approximately 500m).

### 2.2. Isotopic and chemical analysis

The laboratory analysis of water-soluble inorganic ions (including $Cl^-$, $NO_3^-$, $SO_4^{2-}$, $Na^+$, $NH_4^+$, $K^+$, $Mg^{2+}$, etc.) and the dual isotopic composition of $NO_3^-$ ($\delta^{18}O$ and $\delta^{15}N$) was conducted in Jiangxi Province Key Laboratory of the Causes and Control of Atmospheric Pollution, East China University of Technology and the analytical procedure can be found in our previous work (Guo et al., 2020; Zhang et al., 2020a). Briefly, the major inorganic chemical species in the $PM_{2.5}$ samples were extracted using ultrapure water (Millipore, 18.2MΩ) and the extract solutions were filtered. Inorganic ions in the extract solutions were determined using routine chemical methods (Guo et al., 2020). The bacterial approach was used to quantify the $\delta^{15}N$ and $\delta^{18}O$ values of $NO_3^-$ (Casciotti et al., 2002; Fang et al., 2011a; Sigman et al., 2001; Liu et al., 2018). The bacteria *Pseudomonas aureofaciens* (ATCC 13985#) without $N_2O$ reductase was able to turn the $NO_3^-$ into gaseous $N_2O$ quantitatively with very little impaction on the $\delta^{18}O$ values of substrate $NO_3^-$ (Hastings, 2004; Hastings et al., 2003). The gaseous $N_2O$ was then introduced to a continuous-flow isotope ratio mass spectrometer coupled with Gasbench-II for $\delta^{15}N$ and $\delta^{18}O$ determination. The reported data was first calibrated using international recognized nitrate standards (USGS32, USGS34, USGS35, IAEA-NO3) with certified $\delta^{18}O$ and $\delta^{15}N$ values and presented using the δ notation (in units of per mil, ‰) as follows in this study:

$$\delta^{18}O–NO_3^- = [(^{18}O/^{16}O)_{sample}/(^{18}O/^{16}O)_{VSMOW} - 1] \times 1000$$

$$\delta^{15}N–NO_3^- = [(^{15}N/^{14}N)_{sample}/(^{15}N/^{14}N)_{N2\ in\ air} - 1] \times 1000$$

The presented $\delta^{15}N–NO_3^-$ values were also corrected for the contribution of mass-independent $^{14}N–^{14}N–^{17}O$ to the analyst $N_2O$, because the aerosol $NO_3^-$ has substantial mass-independent $^{17}O$ anomaly (Hastings, 2004; Hastings et al., 2003). Due to the unavailable of $\delta^{17}O$ determinations in our laboratory at present, published relationships between $\delta^{18}O$ and $\Delta^{17}O$ were used in this study (Hastings, 2004; Hastings et al., 2003; Michalski et al., 2003; Wang et al., 2019). The standard deviations of 20 replicate injections of international standards were better than ±0.2‰ for $\delta^{15}N$ and ±0.5‰ for $\delta^{18}O$. Concentrations of $NO_2^-$ were usually smaller than the $NO_3^-$ by two orders of magnitude and therefore did not impact the isotopic composition of $NO_3^-$. More details were included in the Supporting information.

### 2.3. Model simulation of $NO_3$ radical, $N_2O_5$, and aerosol properties

The aerosol acidity and liquid water content (ALWC) were predicted using the thermodynamic model of ISORROPIA-II, which was widely used to describe the aerosol thermodynamic equilibrium, e.g., the gas-to-particle partition of atmospheric nitrate (nitrate partition ration: $\varepsilon_{NO3^-} = NO_3^-/(NO_3^- + HNO_3)$) (Fountoukis and Nenes, 2007; Guo et al., 2015, 2017; Weber et al., 2016). To improve the simulation of aerosol acidity and ALWC, the ISORROPIA-II model was run iteratively until the output particle $NH_4^+$ concentration was very close to the measured one (<1% in this study, Zhang et al., 2020a). Usually, the "S" curve of $\varepsilon_{NO3^-}$ against the predicted pH was used to assess the degree of the gas-to-particle partition of atmospheric nitrate. The performance of ISORROPIA-II has been evaluated elsewhere (Guo et al., 2015, 2017;

Weber et al., 2016). The mixing ratios of $NO_3$ radical and $N_2O_5$ near the sampling sites were simulated using the standard Master Chemical Mechanism (MCM in website http://mcm.leeds.ac.uk/, last access: 3 June 2020), which have been well-presented by Xiao et al. (2020) (e.g., model performance and results). Detailed information on the two models was supported in Text S1.

### 2.4. The theoretical basis of $\delta^{15}N$-$\delta^{18}O$ space of $NO_3^-$ in revealing the different oxidation pathways

As abovementioned (and in Fig. 2), the three nitrate formation pathways were characterized by relatively distinct $\delta^{15}N$-$\delta^{18}O$ signatures (Walters and Michalski, 2016; Liu et al., 2020). The isotopic fractionation associated with the three pathways has been theoretically determined and supported in Text S2 in detail. Assuming $\delta^{15}N\text{-}NOx = 0$ and T = 273.2K, the endmember value of $\delta^{15}N\text{–}NO_3^-$ through OH channel was approximately 7.9 ± 3.1‰ (e.g., kinetic fractionation factor of OH oxidation was ignored, isotope equilibrium fractionation factor between NO and $NO_2$ ranged from 42‰ to 45‰, isotope equilibrium fractionation factor from gaseous $HNO_3$ to particle $NO_3^-$ was minor since the $\varepsilon_{NO3\text{-}}$ approximately 100% for the most of time, the fraction of $NO_2$ to NO*x* ($f_{NO2}$, Fig. S3) was from 0.70 to 0.95, see Text S2 for detailed explanations), the endmember value of $\delta^{15}N\text{–}NO_3^-$ through $N_2O_5$ hydrolysis channel was approximately +29.4 ± 1.1‰ and that through $NO_3$+HC pathway was roughly −18.7 ± 1.1‰; in comparison, the endmember value of $\delta^{18}O\text{–}NO_3^-$ generated through $NO_3$+HC and $N_2O_5$ pathway compared well, on average of +92 ± 9.5‰, while that through $NO_2$+OH channel approximated +55‰ (Fang et al., 2011a). Therefore, the $\delta^{18}O\text{–}NO_3^-$ signatures can be used to distinguish the contribution of daytime and nocturnal channels ($NO_3$+HC and $N_2O_5$ hydrolysis), despite with nonnegligible uncertainty. Furthermore, the daily $\delta^{15}N$ and $\delta^{18}O$ values of $NO_3^-$ should be within the triangle region restricted by the theoretical endmember values of $\delta^{15}N$-$\delta^{18}O$ of $NO_3^-$ (Fig. 2). To assess the relative contribution of the three different pathways, we further assumed the complete mixing of $NO_3^-$ formed through daytime and nocturnal pathways. Consequently, a linear regression was anticipated between the $\delta^{15}N\text{–}NO_3^-$ against the corresponding $\delta^{18}O\text{–}NO_3^-$ with the slope determined by the relative importance of $NO_3$+HC channel in the overall nocturnal pathways (Fig. 2). Simply, the slope of $\delta^{15}N\text{–}NO_3^-$ against the $\delta^{18}O\text{–}NO_3^-$ was approximately 0.54 with the absence of $NO_3$+HC channel, while the slope approximated −0.65 with the absence of $N_2O_5$ hydrolysis pathway (Fig. 2). The slope was, therefore, regarded as the additional strong constraint on apportioning the relative contribution of the two nocturnal pathways.

## 3. Results and discussion

### 3.1. Temporal evolution of $PM_{2.5}$ $NO_3^-$ and relevant parameters

Fig. 3 depicted the time series of $NO_3^-$ in $PM_{2.5}$ and the relevant parameters, especially those impacted the accumulation of $NO_3^-$ (e.g., T, RH, and particle pH). The temperature was gradually decreased with time, while the RH varied widely, from 30% to 95%. Consistent with previous reports, the concentrations of $NO_3^-$ exhibited large variability during the campaign, ranged from 2.8 μg/m$^3$ to 57.7 μg/m$^3$ (on average of 20.5 ± 10.4 μg/m$^3$). The mean concentration of $NO_3^-$ in the wintertime of Nanchang city was observed to be in line with that in nearby urban cities, e.g., Changsha (19.4 μg/m$^3$ from September 2013 to August 2014, Zhang et al., 2020), Wuhan (23.9 μg/m$^3$ in winter 2019, Zheng et al., 2020) and Nanjing (16.7 μg/m$^3$ from March 2016 to August 2017, Lin et al., 2020). Furthermore, the loadings of particulate $NO_3^-$ were higher than that of $SO_4^{2-}$ (range: 2.7–30.2 μg/m$^3$; mean:11.9 ± 5.2 μg/m$^3$), especially during haze episodes (Fig. 3). In fact, the ratio of $NO_3^-$ to $SO_4^{2-}$ ($NO_3^-/SO_4^{2-}$) increased from clean periods (<1.0) to polluted days (>2.0, Fig. S2), on average of 1.8 during the whole observations, which was even higher than that in polluted northern city environments (e.g., 1.4 in Beijing of winter 2016 (Xu et al., 2019), 1.6 in several cities surrounded North China Plain in winter 2017 (Fu et al., 2020)). These results may suggest the increasing importance of $NO_3^-$ in the haze development in southern urban cities of China, which has been recorded as a distinct feature over China. Other major ions, such as $NH_4^+$ presented parallel trends to the evolution of $NO_3^-$ (Fig. 3).

Theoretically, the buildup of particulate $NO_3^-$ highly depends on two subprocesses: the oxidation of NO*x* to $HNO_3$ and the thermodynamic equilibrium partition between $HNO_3$ and $NO_3^-$ (Seinfeld and Pandis, 2016; Zhang et al., 2020c). Usually, the gas-to-particle partition of

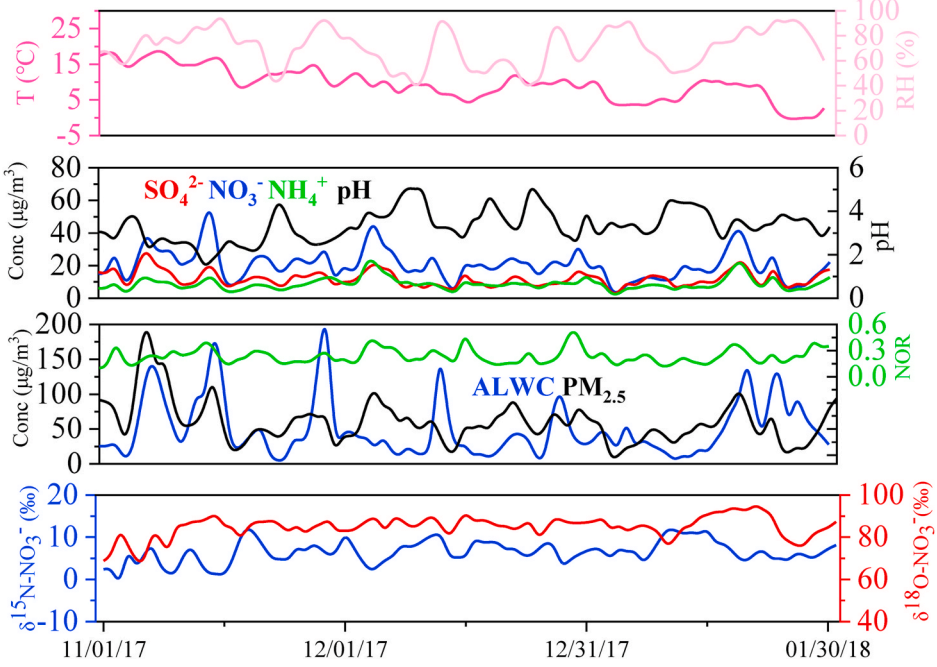


**Fig. 3.** Temporal evolution of meteorological variables including RH and T, mass concentrations of major inorganic chemical species in PM2.5, NOR (NO*x* oxidation ratio), the aerosol properties (acidity and aerosol water content) and the dual isotopic compositions of nitrate in PM2.5 in winters of 2017–2018 in urban Nanchang.

atmospheric nitrate is closely related to the availability of gaseous $NH_3$, the variations in RH and temperature (Chen et al., 2020; Guo et al., 2015; Li et al., 2018; Sun et al., 2018). In the present study, the degree of nitrate partition ratio ($\varepsilon_{NO3-}$) was estimated using the aerosol pH, which was predicted by the thermodynamic model of ISORROPIA-II, since the ambient measurements of gaseous $NH_3$ and $HNO_3$ were unavailable during the campaign. As indicated by the S curve of $\varepsilon_{NO3-}$ (Fig. 4), the atmospheric nitrate overwhelming existed in the particle phase, reflected by the relatively moderate pH of $PM_{2.5}$ (mean of 3.3, mode of 2.5). This was consistent with the observations that abundant $NH_3$ in the urban environment facilitated the partition of atmospheric nitrate into the particle phase (Chang et al., 2019b; Guo et al., 2018). The aerosol pH generally exhibited declining trends with the accumulation of $NO_3^-$, with a pH of approximately 1.5 during extreme nitrate polluted period ($\varepsilon_{NO3-}$ corresponded to be 0.70, Figs. 3 and 4), suggesting a high ambient gaseous $HNO_3$ concentration when haze occurred. Although, these results indicated that the $HNO_3$ formation was the key process that determined the accumulation of particle $NO_3^-$ in the wintertime of Nanchang city, which resembled that in northern urban environments of China (Fu et al., 2020; Wen et al., 2018; Yan et al., 2019). For instance, Fu et al. (2020) confirmed that the increased conversion ratio of NO*x* to $HNO_3$ was the cause of the subdued response of $NO_3^-$ to NO*x* emission reduction in urban environments around the North China Plain (Fu et al., 2020). During the observations, the NOR (nitrogen oxidation ratio) varied significantly (from 0.10 to 0.52, mean of 0.24 ± 0.10), and generally increased with the haze development (Fig. 3). In contrast, the gaseous precursors of $NO_2$ and $O_3$ generally declined when haze pollution occurred, while the simulated concentrations of $NO_3$ radical and $N_2O_5$ elevated with the haze development (Fig. S4). Together, results identified that the efficient secondary transformation was the driving factor that regulating nitrate aerosol pollution in the winter of urban Nanchang.

### 3.2. Signatures of $\delta^{18}O$–$NO_3^-$ and $\delta^{15}N$–$NO_3^-$ under different nitrate regimes

During the observations, the daily $\delta^{15}N$–$NO_3^-$ values varied significantly, ranged from −1.9‰ to +12.5‰ with a mean value of +6.5 ± 3.7‰ (Fig. 3). The $\delta^{15}N$–$NO_3^-$ values of $PM_{2.5}$ in winter Nanchang were in the range of that reported in winter Shanghai (approximately +7.5‰ in 2013, +8.9‰ in 2016) and Guangzhou (approximately +7.5‰ in 2013; Zong et al., 2020), while lower than that in a nearby urban city of Wuhan (approximately +13‰ in 2013; Zong et al., 2020), the northern megacity of Beijing (+11.9‰ in 2014; Song et al., 2019) and Tianjin (+14.1‰ in 201; Feng et al., 2020). Meanwhile, the values of $\delta^{18}O$–$NO_3^-$ (+85.9 ± 17.7‰) in $PM_{2.5}$ during our campaign ranged widely from +69.1‰ to +95.5‰, which were also well within the broad ranges reported in previous studies conducted in the northern hemisphere (Feng et al., 2020; He et al., 2020; Michalski, 2005; Michalski et al., 2012; Savarino et al., 2016; Wankel et al., 2010; Xiao et al., 2020; Yang et al., 2014; Zong et al., 2020). However, the mean value of $\delta^{18}O$–$NO_3^-$ in winter Nanchang was generally smaller than that in Shanghai and Wuhan (both approximately +100‰ in winter 2013; Zong et al., 2020), but compared well with that in Beijing (+84.8‰ in winter 2013; Wang et al., 2019) and Tianjin (+85.1‰ and +83.4‰ in January 2017 and 2018, respectively; Feng et al., 2020). Monthly, the $\delta^{15}N$–$NO_3^-$ values gradually increased from November to January, with values of +5.2 ± 3.3‰, +6.9 ± 2.5‰ and +7.3 ± 2.5‰, respectively, which was consistent with previous reports that $NO_3^-$ in $PM_{2.5}$ was usually $^{15}N$-enriched in cold seasons than in warm periods (Gobel et al., 2013; Zong et al., 2017). In comparison, no obvious temporal trend was observed for $\delta^{18}O$–$NO_3^-$.

Simple comparison of $\delta^{15}N$–$NO_3^-$ in $PM_{2.5}$ among different seasons or urban environment traits are maybe of finite in extending our understandings of the diversity of atmospheric $NO_3^-$ nitrogen signatures, since the $\delta^{15}N$–$NO_3^-$ in $PM_{2.5}$ was suggested as a comprehensive result of numerous drivers, e.g., source characteristics of NO*x*, the isotopic exchange between NO and $NO_2$, kinetic isotopic fractionation during NO*x* conversion to $HNO_3$, Rayleigh-controlled isotopic fractionation with $NO_3^-$ accumulation and the potential equilibrium exchange between $HNO_3$ and $NO_3^-$, to the best of our knowledge. Interestingly, the $\delta^{15}N$–$NO_3^-$ presented a negative correlation with the corresponding $NO_3^-$ concentrations, though not significant (Fig. S5), which implies that particulate $NO_3^-$ may originate from different sources or generate from different pathways during the severe nitrate aerosol polluted episode (Fan et al., 2020). Meanwhile, the $\delta^{18}O$–$NO_3^-$ increased significantly with the increasing $NO_3^-$ concentrations (Fig. S5). This indicated both the $\delta^{15}N$–$NO_3^-$ and $\delta^{18}O$–$NO_3^-$ were related to the nitrate accumulation, to a large extent, and can be used to infer the relative importance of different channels. For clarity, we compared the $\delta^{15}N$–$NO_3^-$ and $\delta^{18}O$–$NO_3^-$ under different nitrate regimes (e.g., <5 μg/m$^3$, 5–10 μg/m$^3$, 10–15 μg/m$^3$, etc., as presented in Fig. 5) to assess the ability of the dual-isotope signatures in revealing the nitrate formation pathways. As stated, the $\delta^{18}O$–$NO_3^-$ increased with the buildup of $NO_3^-$ (except for the nitrate regime of 25–30 μg/m$^3$), while the $\delta^{15}N$–$NO_3^-$ increased until $NO_3^-$

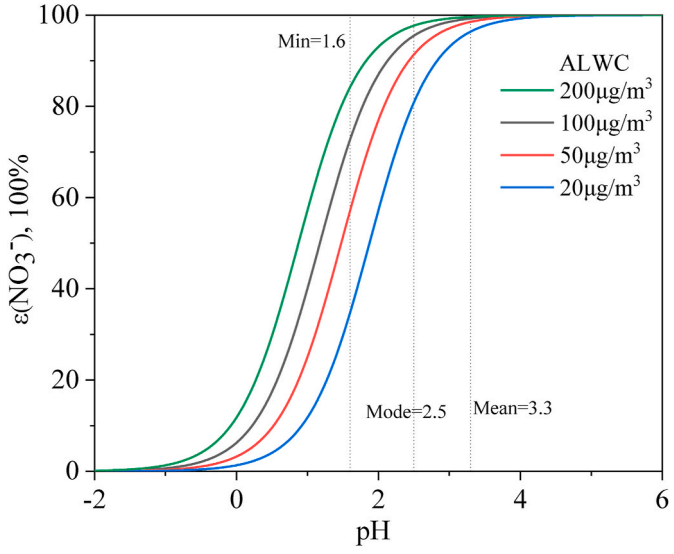


**Fig. 4.** S curves of ε($NO_3^-$) plotted against ISORROPIA-predicted pH. The aerosol water content (ALWC) was set as 20, 50, 100 and 200 μg/m$^3$, respectively.

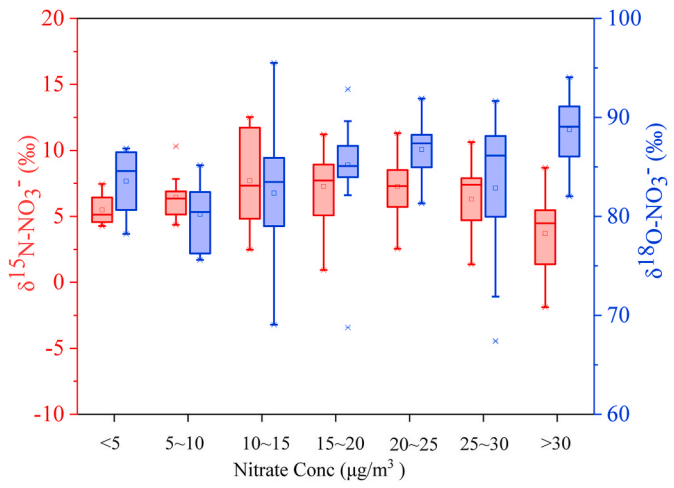


**Fig. 5.** The dual isotopic signatures of nitrate under different nitrate regimes. Apparently, the $\delta^{15}N$–$NO_3^-$ values declined significantly when nitrate concentrations higher than 20 μg/m$^3$.

reached up to 25 μg/m$^3$ (+5.5‰ to +7.3‰) and then decreased considerably (+7.3‰ to +4.0‰) as $NO_3^-$ continued to ascend (25–57.6 μg/m$^3$). The parallel increments of $\delta^{18}O$–$NO_3^-$ and $\delta^{15}N$–$NO_3^-$ before $NO_3^-$ accumulated to 25 μg/m$^3$ may indicate the dominance of $N_2O_5$ hydrolysis in $NO_3^-$ generation, since this channel was associated with $^{15}N$ and $^{18}O$ enriched signatures (Walters and Michalski, 2016). The importance of $N_2O_5$ heterogeneous uptake on the aerosol surface in the fast development of nitrate aerosol across China has been well confirmed in previous researches (Chen et al., 2018; Mitroo et al., 2019; Wang et al., 2017; Yan et al., 2019). However, the opposite variation tendency between $\delta^{15}N$–$NO_3^-$ and $\delta^{18}O$–$NO_3^-$ under the extreme nitrate aerosol pollution regimes (e.g., 25–57.6 μg/m$^3$) may suggest the potential contribution of $NO_3$+HC channel in the nitrate formation. In addition, the $\delta^{15}N$–$NO_3^-$ values exhibited negative correlations with the ratio of $NO_3/N_2O_5$ (or $NO_3/NO_2$) during the observations, further implying the contribution of $NO_3$+HC pathways in nitrate production, to some extent (Fig. S6). Overall, these results preliminary suggested the potential capacity of $\delta^{15}N$–$NO_3^-$ in elucidating the NO*x* oxidation chemistry.

### 3.3. Relative contribution of specific-pathway in nitrate production of wintertime Nanchang

Throughout the winter campaign, no obvious correlation was observed between $\delta^{15}N$–$NO_3^-$ and $\delta^{18}O$–$NO_3^-$ in urban Nanchang (Fig. 6 A). A similar phenomenon between $\delta^{15}N$–$NO_3^-$ and $\delta^{18}O$–$NO_3^-$ or $\Delta^{17}O$–$NO_3^-$ has been reported in previous studies in the coastal megacity of Shanghai and Guangzhou (He et al., 2018; Su et al., 2020), an island in Bohai (Zong et al., 2017) and marine boundary layer (Morin et al., 2009; Savarino et al., 2013), while other reports suggested aforementioned correlations may be positive (for $PM_{2.5}$ in Beijing, Song et al., 2019; dry deposition in several CASTNET sites of USA, Elliott et al., 2009) or negative (e.g., polar sites, Morin et al., 2008; Savarino et al., 2016; marine island, Altieri et al., 2013; Yang et al., 2014). It appeared that the $\delta^{15}N$–$NO_3^-$ increased with the increasing of $\delta^{18}O$–$NO_3^-$ or $\Delta^{17}O$–$NO_3^-$ in inland environments, while $\delta^{15}N$–$NO_3^-$ changed little or even decreased with the increment of $\delta^{18}O$–$NO_3^-$ or $\Delta^{17}O$–$NO_3^-$ in marine or coastal environments, despite with a few exceptions. We inferred that the $N_2O_5$ hydrolysis channel was responsible for the positive correlations between the N and O isotopic composition of $NO_3^-$ in inland environments, while the participant of $NO_3$+HC or $NO_3$+DMS channels, of which the endmember was registered as $^{15}N$-depleted but $^{18}O$-enriched values resulted in relatively negative $\delta^{15}N$–$NO_3^-$ values when $\delta^{18}O$–$NO_3^-$ values (or $NO_3^-$ concentrations) increased. Therefore, results that the distribution tendency corresponds to case II in Fig. 2 may indicate that the $NO_3$+HC channel contributed to the $NO_3^-$ accumulation in the inland urban city of Nanchang, to a large extent.

However, we also realized that the Rayleigh-controlled fractionation effect was also responsible for the $^{15}N$-depleted $NO_3^-$ in the regime of $NO_3^-$ concentrations higher than 30 μg/m$^3$ (corresponding to rapid nitrate accumulation stage). In the rapid-growth stage of particulate $NO_3^-$, the $\delta^{15}N$–$NO_3^-$ should be gradually decreased with time (Fig. S7). Assuming the overall nitrogen isotopic fractionation effect (ε) approximated 10.0‰ and initial $\delta^{15}N$-NO*x* = 0‰, values of $\delta^{15}N$–$NO_3^-$ should become less positive from +10‰ initially to +7.7‰ when NOR reached up to 0.4 (the remaining fraction of NO*x* was 0.6, corresponding to $NO_3^-$ concentration of 30 μg/m$^3$, Fig. 3). To alleviate the Rayleigh-driven $^{15}N$-depleted effect on $\delta^{15}N$–$NO_3^-$, strategies of either data with $NO_3^-$ concentration higher than 30 μg/m$^3$ (n = 15) were removed or all data was rectified for Rayleigh fractionation effect were applied in the following discussion. As presented in Fig. 6 (A, B, and C), no obvious correlations and resemble distribution in biplot of dual-isotopic mixing space were observed under each scenario, which further indicated the importance of the $NO_3$+HC channel in nitrate accumulation in urban Nanchang.

To quantify the relative contribution of individual oxidation pathways, an alternative approach based on the $\delta^{15}N$-$\delta^{18}O$ space of $NO_3^-$ was presented in this study (see Material and Method). The fractional contribution of OH oxidation channel to $NO_3^-$ production based on the $\delta^{18}O$ approach fluctuated widely during the campaign, from less than 10% in heavily nitrate polluted days to approximately 70% in clean periods, with a mean of 30.4 ± 14.3% (Fig. 7). The broad range can be attributed to the distinct daily atmospheric conditions during the observation period. The possible fractional contribution of nocturnal channels correspondingly accounted for 69.6 ± 14.3%. Results directly suggested the dominance of nocturnal chemistry in nitrate production in winter seasons of urban environments, consistent with previous reports

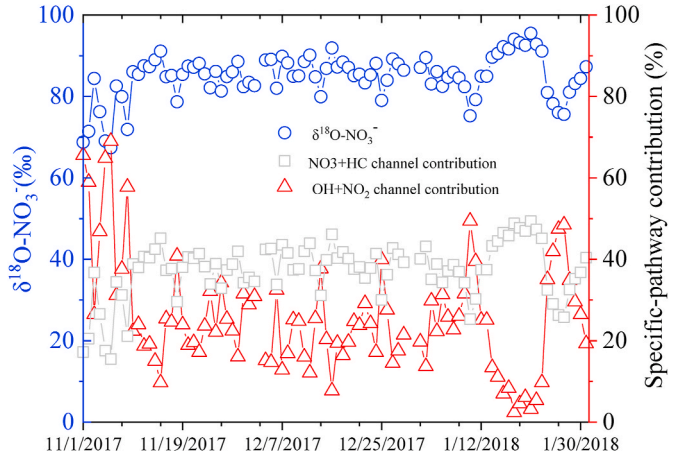


**Fig. 7.** Specific pathway contribution to nitrate formation during the campaign.

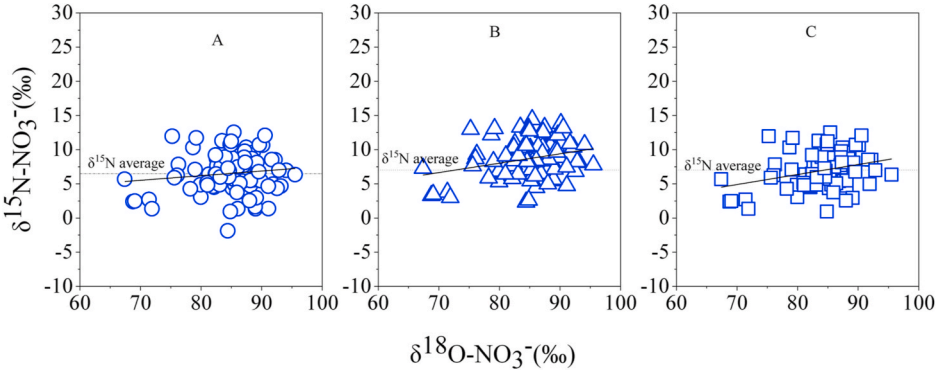


**Fig. 6.** Correlations between $\delta^{15}N$–$NO_3^-$ and $\delta^{18}O$–$NO_3^-$ values under different scenarios: A) original data; B) data corrected for Rayleigh effect; C) data with nitrate concentration higher than 30 μg/m$^3$ were removed. Clearly, on correlations were observed between $\delta^{15}N$–$NO_3^-$ and $\delta^{18}O$–$NO_3^-$ values.

(He et al., 2018; Luo et al., 2019; Wang et al., 2017; Yan et al., 2019). The relative importance of $N_2O_5$ hydrolysis and $NO_3$+HC channel was further quantified according to the regression slopes of $\delta^{15}N$–$NO_3^-$ against $\delta^{18}O$–$NO_3^-$. As elucidated in Fig. 2, the $NO_3$+HC channel may contribute to the nocturnal nitrate accumulation in urban Nanchang in much the same level that $N_2O_5$ hydrolysis contributed, as $\delta^{15}N$–$NO_3^-$ did not correlate with $\delta^{18}O$–$NO_3^-$ (slope, therefore, assumed to be 0). The fractional contribution of the $NO_3$+HC channel was calculated to range from 14.2% to 45.5%, on average of 32.8% during the campaign, which emphasized the unignorable role of $NO_3$ radical chemistry in nitrate formation in winter Nanchang. In contrast, numerous researches suggested the minor role of the $NO_3$+HC channel in nitrate accumulation in the inland city (He et al., 2018; Michalski et al., 2003). For instance, Alexzander et al. (2020) predicted that the $NO_3$+HC channel only accounted for 4–5% of the $NO_3^-$ accumulation globally (Alexander et al., 2019). Further, particulate $NO_3^-$ was generated only when $NO_3$ radical reacted with saturated hydrocarbons but the rate constants were relatively slow (e.g., in the order of $10^{-16}$ $cm^3$ $molecule^{-1}$ $s^{-1}$), while organic nitrate was produced when $NO_3$ radical reacted with unsaturated hydrocarbons (i.e., isoprene, rate constants was in the order of $10^{-13}$ $cm^3$ $molecule^{-1}$ $s^{-1}$), which may account for 20% of the total nitrates (Ng et al., 2008). Although, our calculation of the contribution of $NO_3$+HC channel (32.8%) was consistent with the corresponding results of specific-pathways contribution in winter Beijing (34 ± 10%, in winter 2014) estimated using $\Delta^{17}O$–$NO_3^-$ (Wang et al., 2019). Another possible reason for the high contribution of $NO_3$+HC channel in nitrate production was that the organic nitrate produced via $NO_3$ radical reacted with alkanes may be transformed into inorganic nitrate during the pretreatment processes or the organic nitrate was also converted into gaseous $N_2O$ by the denitrifier bacteria (Lockwood et al., 2008). The hypothesis was based on the fact that the atmospheric organic oxidized nitrogen can be absorbed by foliage and incorporated into amino acids (Lockwood et al., 2008), however, no such test of whether the organic nitrogen can be chemically (or biologically) converted into inorganic one during routine laboratory pretreatment was conducted at present, to the best of our knowledge. Therefore, a solid conclusion on the specific-pathways contribution to $NO_3^-$ formation was hard to draw; however, our results may infer the non-negligible contribution of the $NO_3$+HC pathway in nitrate generation in the wintertime of urban Nanchang.

## 4. Conclusion

Particulate nitrate has been observed as a major component of $PM_{2.5}$ in the urban environment in China. A better understanding regarding the contribution of different chemical pathways to the production of $NO_3^-$ is therefore crucial for mitigation $PM_{2.5}$ pollution in the future. In the present study, daily $PM_{2.5}$ samples were collected in the wintertime of urban Nanchang and the related parameters (e.g., $NO_3^-$ concentration, dual isotopic signature, precursors concentrations) were determined to quantify the chemical conversion of $NO_3^-$. Concentrations of nitrate ranged from 2.8 μg/$m^3$ to 57.7 μg/$m^3$, with a mean of 20.5 ± 10.4 μg/$m^3$, making the nitrate an important component that driven the haze appearance during the observation period. To distinguish the relative contribution of three major oxidation pathways, a simple but robust approach was used in this study. Briefly, the environmental significance of $\delta^{15}N$-$\delta^{18}O$ space of $NO_3^-$ was defined, which performed excellently in partition the relative importance of $NO_3$+HC and $N_2O_5$ hydrolysis channels. Taking full advantage of this approach, our results suggested the considerable contribution of $NO_3$+HC in nitrate production (average of 32.8%), even reached up to 45.5% on extremely polluted days. Although with a certain defect, our result provided an alternative perspective to better understanding nitrate chemistry in the polluted urban environment.

To date, explanations on the variability of $\delta^{15}N$–$NO_3^-$ is still less well-established. The ambient $\delta^{15}N$–$NO_3^-$ was usually regarded as a hybrid of $\delta^{15}N$ of the source NO*x*, the isotopic effect of the Leighton cycle, the fractionation effect associated with the oxidation reaction ($NOx \rightarrow HNO_3$) and partition process ($HNO_3 \leftrightharpoons NO_3^-$), and possible the deposition influence. Our analysis suggested that certain neglected processes also significantly affected the signatures of $\delta^{15}N$–$NO_3^-$, e.g., the Rayleigh type fractionation during the rapid haze development period and the potential gas-to-particle exchange of atmospheric nitrate. Both the fractionation effects have been reported previously and may affect the source appointment of NO*x*, to a certain extent. Furthermore, the interference of organic nitrates ($RONO_2$) to the isotopic composition of inorganic nitrate during laboratory analysis should be tested in the future. Nevertheless, $\delta^{15}N$–$NO_3^-$ was still a robust regional indicator for revealing the NO*x* source.

## CRediT author contribution statement

**Zhongyi Zhang:** Conceptualization, Software, Investigation, Writing – original draft. **Lin Cao:** and. **Yue Liang:** Methodology, Resources, Writing – review & editing, Data curation. **Hui Guan:** Software, Investigation, Writing – original draft. **Nengjian Zheng:** Conceptualization, Resources, Writing – review & editing, Data curation.

## Declaration of competing interest

The authors declare that they have no conflicts of interest.

## Acknowledgments

This work was supported by the National Natural Science Foundation of China (Grant no. 41863001 and 41425014). Data used in this paper are available upon request from the corresponding author (zhengnengjian@ecut.edu.cn).

## Appendix A. Supplementary data

Supplementary data to this article can be found online at https://doi.org/10.1016/j.atmosenv.2021.118387.

## References

Alexander, B., Hastings, M., Allman, D., Dachs, J., Thornton, J., Kunasek, S., 2009. Quantifying atmospheric nitrate formation pathways based on a global model of the oxygen isotopic composition ($\Delta^{17}O$) of atmospheric nitrate. Atmos. Chem. Phys. 9, 5043–5056.

Alexander, B., Sherwen, T., Holmes, C., Fisher, J., Chen, Q., Evans, M., Kasibhatla, P., 2019. Global inorganic nitrate production mechanisms: comparison of a global model with nitrate isotope observations. Atmos. Chem. Phys. 1–36.

Altieri, K., Hastings, M., Gobel, A., Peters, A., Sigman, D.M., 2013. Isotopic composition of rainwater nitrate at Bermuda: the influence of air mass source and chemistry in the marine boundary layer. J. Geophys. Res. Atmos. 118 (11), 304–311, 316.

An, Z., Huang, R.-J., Zhang, R., Tie, X., Li, G., Cao, J., Zhou, W., Shi, Z., Han, Y., Gu, Z., Ji, Y., 2019. Severe haze in northern China: a synergy of anthropogenic emissions and atmospheric processes. Proc. Nat. Acad. Sci. U.S.A. 116, 8657–8666.

Casciotti, K.L., Sigman, D.M., Hastings, M.G., Böhlke, J., Hilkert, A., 2002. Measurement of the oxygen isotopic composition of nitrate in seawater and freshwater using the denitrifier method. Anal. Chem. 74, 4905–4912.

Chang, Y., Zhang, Y.-L., Li, J., Tian, C., Song, L., Zhai, X., Zhang, W., Huang, T., Lin, Y.-C., Zhu, C., Fang, Y., Lehmann, M.F., Chen, J., 2019a. Isotopic constraints on the atmospheric sources and formation of nitrogenous species in clouds influenced by biomass burning. Atmos. Chem. Phys. 19, 12221–12234.

Chang, Y., Zou, Z., Zhang, Y., Deng, C., Hu, J., Shi, Z., Dore, A.J., Collett, J., 2019b. Assessing contributions of agricultural and non-agricultural emissions to atmospheric ammonia in a Chinese megacity. Environ. Sci. Technol. 53, 1822–1833.

Chen, X., Wang, H., Lu, K., Li, C., Zhai, T., Tan, Z., Ma, X., Yang, X., Liu, Y., Chen, S., 2020. Field determination of nitrate formation pathway in winter beijing. Environ. Sci. Technol.

Chen, Y., Wolke, R., Ran, L., Birmili, W., Spindler, G., Schröder, W., Su, H., Cheng, Y., Tegen, I., Wiedensohler, A., 2018. A parameterization of the heterogeneous hydrolysis of $N_2O_5$ for mass-based aerosol models: improvement of particulate nitrate prediction. Atmos. Chem. Phys. 18, 673–689.

Elliott, E.M., Kendall, C., Boyer, E.W., Burns, D.A., Lear, G.G., Golden, H.E., Harlin, K., Bytnerowicz, A., Butler, T.J., Glatz, R., 2009. Dual nitrate isotopes in dry deposition: utility for partitioning NOx source contributions to landscape nitrogen deposition. J. Geophys. Res. Atmos. 114.

Fan, M.Y., Zhang, Y.L., Lin, Y.C., Cao, F., Zhao, Z.Y., Sun, Y., Qiu, Y., Fu, P., Wang, Y., 2020. Changes of emission sources to nitrate aerosols in Beijing after the clean air actions: evidence from dual isotope compositions. J. Geophys. Res. Atmos. 125 e2019JD031998.
Fang, Y., Koba, K., Makabe, A., Takahashi, C., Zhu, W., Hayashi, T., Hokari, A.A., Urakawa, R., Bai, E., Houlton, B.Z., 2015. Microbial denitrification dominates nitrate losses from forest ecosystems. Proc. Nat. Acad. Sci. U.S.A. 112, 1470–1474.
Fang, Y., Koba, K., Wang, X., Wen, D., Li, J., Takebayashi, Y., Liu, X., Yoh, M., 2011a. Anthropogenic imprints on nitrogen and oxygen isotopic composition of precipitation nitrate in a nitrogen-polluted city in southern China. Atmos. Chem. Phys. 11, 1313.
Fang, Y., Yoh, M., Koba, K., Zhu, W., Takebayashi, Y., Xiao, Y., Lei, C., Mo, J., Zhang, W., Lu, X., 2011b. Nitrogen deposition and forest nitrogen cycling along an urban–rural transect in southern China. Global Change Biol. 17, 872–885.
Felix, J.D., Elliott, E.M., 2014. Isotopic composition of passively collected nitrogen dioxide emissions: vehicle, soil and livestock source signatures. Atmos. Environ. 92, 359–366.
Felix, J.D., Elliott, E.M., Shaw, S.L., 2012. Nitrogen isotopic composition of coal-fired power plant NOx: influence of emission controls and implications for global emission inventories. Environ. Sci. Technol. 46, 3528–3535.
Feng, X., Li, Q., Tao, Y., Ding, S., Chen, Y., Li, X.D., 2020. Impact of Coal Replacing Project on atmospheric fine aerosol nitrate loading and formation pathways in urban Tianjin: insights from chemical composition and $^{15}N$ and $^{18}O$ isotope ratios. Sci. Total. Environ. 708, 134797.
Fountoukis, C., Nenes, A., 2007. Isorropia II: a computationally efficient thermodynamic equilibrium model for $K^+$–$Ca^{2+}$–$Mg^{2+}$–$NH_4^+$–$Na^+$–$SO_4^{2-}$–$NO_3^-$–$Cl^-$–$H_2O$ aerosols. Atmos. Chem. Phys. 7, 4639–4659.
Fu, X., Wang, T., Gao, J., Wang, P., Liu, Y., Wang, S., Zhao, B., Xue, L., 2020. Persistent heavy winter nitrate pollution driven by increased photochemical oxidants in northern China. Environ. Sci. Technol. 54, 3881–3889.
Geng, G., Xiao, Q., Zheng, Y., Tong, D., Zhang, Y., Zhang, X., Zhang, Q., He, K., Liu, Y., 2019. Impact of China's air pollution prevention and control action plan on $PM_{2.5}$ chemical composition over eastern China. Sci. China Earth Sci. 1–13.
Geng, L., Alexander, B., Cole-Dai, J., Steig, E.J., Savarino, J., Sofen, E.D., Schauer, A.J., 2014. Nitrogen isotopes in ice core nitrate linked to anthropogenic atmospheric acidity change. Proc. Nat. Acad. Sci. U.S.A. 111, 5808–5812.
Gobel, A.R., Altieri, K.E., Peters, A.J., Hastings, M.G., Sigman, D.M., 2013. Insights into anthropogenic nitrogen deposition to the North Atlantic investigated using the isotopic composition of aerosol and rainwater nitrate. Geophys. Res. Lett. 40, 5977–5982.
Guo, H., Liu, J., Froyd, K.D., Roberts, J.M., Veres, P.R., Hayes, P.L., Jimenez, J.L., Nenes, A., Weber, R.J., 2017. Fine particle pH and gas–particle phase partitioning of inorganic species in Pasadena, California, during the 2010 CalNex campaign. Atmos. Chem. Phys. 17, 5703–5719.
Guo, H., Otjes, R., Schlag, P., Kiendler-Scharr, A., Nenes, A., Weber, R.J., 2018. Effectiveness of ammonia reduction on control of fine particle nitrate. Atmos. Chem. Phys. 18, 12241–12256.
Guo, H., Xu, L., Bougiatioti, A., Cerully, K.M., Capps, S.L., Hite, J.R., Carlton, A.G., Lee, S. H., Bergin, M.H., Ng, N.L., Nenes, A., Weber, R.J., 2015. Fine-particle water and pH in the southeastern United States. Atmos. Chem. Phys. 15, 5211–5228.
Guo, W., Zhang, Z., Zheng, N., Luo, L., Xiao, H., Xiao, H., 2020. Chemical characterization and source analysis of water-soluble inorganic ions in PM2. 5 from a plateau city of Kunming at different seasons. Atmos. Res. 234, 104687.
Hastings, M.G., 2004. Seasonal variations in N and O isotopes of nitrate in snow at Summit, Greenland: implications for the study of nitrate in snow and ice cores. J. Geophys. Res. Atmos. 109.
Hastings, M.G., Sigman, D.M., Lipschultz, F., 2003. Isotopic evidence for source changes of nitrate in rain at Bermuda. J. Geophys. Res. Atmos. 108.
He, P., Xie, Z., Chi, X., Yu, X., Fan, S., Kang, H., Liu, C., Zhan, H., 2018. Atmospheric $\Delta^{17}O(NO_3^-)$ reveals nocturnal chemistry dominates nitrate production in Beijing haze. Atmos. Chem. Phys. 18, 14465–14476.
He, P., Xie, Z., Yu, X., Wang, L., Kang, H., Yue, F., 2020. The observation of isotopic compositions of atmospheric nitrate in Shanghai China and its implication for reactive nitrogen chemistry. Sci. Total. Environ. 714, 136727.
Li, H., Zhang, Q., Zheng, B., Chen, C., Wu, N., Guo, H., Zhang, Y., Zheng, Y., Li, X., He, K., 2018. Nitrate-driven urban haze pollution during summertime over the North China Plain. Atmos. Chem. Phys. 18, 5293–5306.
Lin, Y.-C., Zhang, Y.-L., Fan, M.-Y., Bao, M., 2020. Heterogeneous formation of particulate nitrate under ammonium-rich regimes during the high-PM2. 5 events in Nanjing, China. Atmos. Chem. Phys. Discuss. 20, 3999–4011.
Liu, X.-Y., Yin, Y.-M., Song, W., 2020. Nitrogen isotope differences between major atmospheric NOy species: implications for transformation and deposition processes. Environ. Sci. Technol. Lett. 7, 227–233.
Liu, X.-Y., Koba, K., Koyama, L.A., Hobbie, S.E., Weiss, M.S., Inagaki, Y., Shaver, G.R., Giblin, A.E., Hobara, S., Nadelhoffer, K., 2018. Nitrate is an important nitrogen source for Arctic tundra plants. Proc. Nat. Acad. Sci. U.S.A. 115, 3398–3403.
Lockwood, A.L., Filley, T.R., Rhodes, D., Shepson, P.B., 2008. Foliar uptake of atmospheric organic nitrates. Geophys. Res. Lett. 35, 386–390.
Luo, L., Wu, Y., Xiao, H., Zhang, R., Lin, H., Zhang, X., Kao, S.-j., 2019. Origins of aerosol nitrate in Beijing during late winter through spring. Sci. Total. Environ. 653, 776–782.
Michalski, G., 2005. Isotopic composition of antarctic dry valley nitrate: implications for NOy sources and cycling in Antarctica. Geophys. Res. Lett. 32.
Michalski, G., Bhattacharya, S., Mase, D.F., 2012. Oxygen isotope dynamics of atmospheric nitrate and its precursor molecules. In: Handbook of Environmental Isotope Geochemistry. Springer, pp. 613–635.
Michalski, G., Scott, Z., Kabiling, M., Thiemens, M.H., 2003. First measurements and modeling of $\Delta^{17}O$ in atmospheric nitrate. Geophys. Res. Lett. 30, 1870.
Mitroo, D., Gill, T.E., Haas, S., Pratt, K.A., Gaston, C., 2019. $ClNO_2$ production from $N_2O_5$ uptake on saline playa dusts: new insights into potential inland sources of $ClNO_2$. Environ. Sci. Technol. 53, 7442–7452.
Morin, S., Savarino, J., Frey, M.M., Domine, F., Jacobi, H.W., Kaleschke, L., Martins, J.M. F., 2009. Comprehensive isotopic composition of atmospheric nitrate in the Atlantic Ocean boundary layer from 65°S to 79°N. J. Geophys. Res. Atmos. 114.
Morin, S., Savarino, J., Frey, M.M., Yan, N., Bekki, S., Bottenheim, J.W., Martins, J.M., 2008. Tracing the origin and fate of NOx in the Arctic atmosphere using stable isotopes in nitrate. Science 322, 730–732.
Ng, N., Kwan, A., Surratt, J., Chan, A., Chhabra, P., Sorooshian, A., Pye, H.O., Crounse, J., Wennberg, P., Flagan, R., 2008. Secondary organic aerosol (SOA) formation from reaction of isoprene with nitrate radicals ($NO_3$). Atmos. Chem. Phys. 8, 4117–4140.
Savarino, J., Morin, S., Erbland, J., Grannec, F., Patey, M.D., Vicars, W., Alexander, B., Achterberg, E.P., 2013. Isotopic composition of atmospheric nitrate in a tropical marine boundary layer. Proc. Nat. Acad. Sci. U.S.A. 110, 17668–17673.
Savarino, J., Vicars, W.C., Legrand, M., Preunkert, S., Jourdain, B., Frey, M.M., Kukui, A., Caillon, N., Roca, J.G., 2016. Oxygen isotope mass balance of atmospheric nitrate at Dome C, East Antarctica, during the OPALE campaign. Atmos. Chem. Phys. 16, 2659–2673.
Seinfeld, J.H., Pandis, S.N., 2016. Atmospheric Chemistry and Physics: from Air Pollution to Climate Change. John Wiley & Sons.
Sigman, D.M., Casciotti, K.L., Andreani, M., Barford, C., Galanter, M., Böhlke, J., 2001. A bacterial method for the nitrogen isotopic analysis of nitrate in seawater and freshwater. Anal. Chem. 73, 4145–4153.
Song, W., Liu, X.-Y., Wang, Y.-L., Tong, Y.-D., Bai, Z.-P., Liu, C.-Q., 2020. Nitrogen isotope differences between atmospheric nitrate and corresponding nitrogen oxides: a new constraint using oxygen isotopes. Sci. Total. Environ. 701, 134515.
Song, W., Wang, Y.-L., Yang, W., Sun, X.-C., Tong, Y.-D., Wang, X.-M., Liu, C.-Q., Bai, Z.-P., Liu, X.-Y., 2019. Isotopic evaluation on relative contributions of major NOx sources to nitrate of $PM_{2.5}$ in Beijing. Environ. Pollut. 248, 183–190.
Song, W., Liu, X.-Y., Hu, C.-C., Chen, G.-Y., Liu, X.-J., Walters, W.W., Michalski, G., Liu, C.-Q., 2021. Important contributions of non-fossil fuel nitrogen oxides emissions. Nat. Commun. 12, 1–7.
Su, T., Li, J., Tian, C., Zong, Z., Chen, D., Zhang, G., 2020. Source and formation of fine particulate nitrate in South China: constrained by isotopic modeling and online trace gas analysis. Atmos. Environ. 231.
Sun, J., Liu, L., Xu, L., Wang, Y., Wu, Z., Hu, M., Shi, Z., Li, Y., Zhang, X., Chen, J., Li, W., 2018. Key role of nitrate in phase transitions of urban particles: implications of important reactive surfaces for secondary aerosol formation. J. Geophys. Res. Atmos. 123, 1234–1243.
Vasilakos, P., Russell, A., Weber, R., Nenes, A., 2018. Understanding nitrate formation in a world with less sulfate. Atmos. Chem. Phys. 18, 12765–12775.
Walters, W.W., Goodwin, S.R., Michalski, G., 2015a. Nitrogen stable isotope composition ($\delta^{15}N$) of vehicle-emitted NOx. Environ. Sci. Technol. 49, 2278–2285.
Walters, W.W., Michalski, G., 2015. Theoretical calculation of nitrogen isotope equilibrium exchange fractionation factors for various NOy molecules. Geochem. Cosmochim. Acta 164, 284–297.
Walters, W.W., Michalski, G., 2016. Theoretical calculation of oxygen equilibrium isotope fractionation factors involving various NO molecules, OH, and $H_2O$ and its implications for isotope variations in atmospheric nitrate. Geochem. Cosmochim. Acta 191, 89–101.
Walters, W.W., Tharp, B.D., Fang, H., Kozak, B.J., Michalski, G., 2015c. Nitrogen isotope composition of thermally produced NOx from various fossil-fuel combustion sources. Environ. Sci. Technol. 49, 11363–11371.
Wang, H., Lu, K., Chen, X., Zhu, Q., Chen, Q., Guo, S., Jiang, M., Li, X., Shang, D., Tan, Z., 2017. High $N_2O_5$ concentrations observed in urban Beijing: implications of a large nitrate formation pathway. Environ. Sci. Technol. Lett. 4, 416–420.
Wang, X., Wang, H., Xue, L., Wang, T., Wang, L., Gu, R., Wang, W., Tham, Y.J., Wang, Z., Yang, L., 2017. Observations of $N_2O_5$ and $ClNO_2$ at a polluted urban surface site in North China: high $N_2O_5$ uptake coefficients and low $ClNO_2$ product yields. Atmos. Environ. 156, 125–134.
Wang, Y.L., Song, W., Yang, W., Sun, X.C., Tong, Y.D., Wang, X.M., Liu, C.Q., Bai, Z.P., Liu, X.Y., 2019. Influences of atmospheric pollution on the contributions of major oxidation pathways to $PM_{2.5}$ nitrate formation in Beijing. J. Geophys. Res. Atmos. 124, 4174–4185.
Wankel, S.D., Chen, Y., Kendall, C., Post, A.F., Paytan, A., 2010. Sources of aerosol nitrate to the Gulf of Aqaba: evidence from δ15N and δ18O of nitrate and trace metal chemistry. Mar. Chem. 120, 90–99.
Weber, R.J., Guo, H., Russell, A.G., Nenes, A., 2016. High aerosol acidity despite declining atmospheric sulfate concentrations over the past 15 years. Nat. Geosci. 9, 282–285.
Wen, L., Xue, L., Wang, X., Xu, C., Chen, T., Yang, L., Wang, T., Zhang, Q., Wang, W., 2018. Summertime fine particulate nitrate pollution in the North China Plain: increasing trends, formation mechanisms and implications for control policy. Atmos. Chem. Phys. 18, 11261–11275.
Womack, C., McDuffie, E., Edwards, P., Bares, R., de Gouw, J., Docherty, K., Dube, W., Fibiger, D., Franchin, A., Gilman, J., 2019. An odd oxygen framework for wintertime ammonium nitrate aerosol pollution in urban areas: NOx and VOC control as mitigation strategies. Geophys. Res. Lett. 46, 4971–4979.
Xiao, H.W., Zhu, R.G., Pan, Y.Y., Guo, W., Zheng, N.J., Liu, Y.H., Liu, C., Zhang, Z.Y., Wu, J.F., Kang, C.A., 2020. Differentiation between nitrate aerosol formation pathways in a southeast Chinese city by dual isotope and modeling studies. J. Geophys. Res. Atmos. 125, e2020JD032604.

Xu, W., Sun, Y., Wang, Q., Zhao, J., Wang, J., Ge, X., Xie, C., Zhou, W., Du, W., Li, J., Fu, P., Wang, Z., Worsnop, D.R., Coe, H., 2019. Changes in aerosol chemistry from 2014 to 2016 in winter in beijing: insights from high-resolution aerosol mass spectrometry. J. Geophys. Res. Atmos. 124, 1132–1147.

Yan, C., Tham, Y.J., Zha, Q., Wang, X., Xue, L., Dai, J., Wang, Z., Wang, T., 2019. Fast heterogeneous loss of $N_2O_5$ leads to significant nighttime NOx removal and nitrate aerosol formation at a coastal background environment of southern China. Sci. Total. Environ. 677, 637–647.

Yang, J.-Y., Hsu, S.-C., Dai, M., Hsiao, S.-Y., Kao, S.-J., 2014. Isotopic composition of water-soluble nitrate in bulk atmospheric deposition at Dongsha Island: sources and implications of external N supply to the northern South China Sea. Biogeosciences 11, 1833.

Yu, Z., Elliott, E.M., 2017. Novel method for nitrogen isotopic analysis of soil-emitted nitric oxide. Environ. Sci. Technol. 51, 6268–6278.

Zhang, N.-N., Guan, Y., Yu, L., Ma, F., Li, Y.-F., 2020. Spatio-temporal distribution and chemical composition of $PM_{2.5}$ in Changsha, China. J. Atmos. Chem. 7, 1–16.

Zhang, Z., Zeng, Y., Zheng, N., Luo, L., Xiao, H., Xiao, H., 2020b. Fossil fuel-related emissions were the major source of $NH_3$ pollution in urban cities of northern China in the autumn of 2017. Environ. Pollut. 113428.

Zhang, Z., Zheng, N., liang, Y., Luo, L., Xiao, H., Xiao, H., 2020c. Dominance of heterogeneous chemistry in summertime nitrate accumulation: insights from oxygen isotope of nitrate ($\delta^{18}O$–$NO_3^-$). ACS. Earth. Space. Chem. 4, 818–824.

Zhang, Z., Zheng, N., Zhang, D., Xiao, H., Cao, Y., Xiao, H., 2020d. Rayleigh based concept to track NOx emission sources in urban areas of China. Sci. Total. Environ. 135362.

Zheng, H., Kong, S., Chen, N., Yan, Y., Liu, D., Zhu, B., Xu, K., Cao, W., Ding, Q., Lan, B., 2020. Significant changes in the chemical compositions and sources of $PM_{2.5}$ in Wuhan since the city lockdown as COVID-19. Sci. Total. Environ. 140000.

Zong, Z., Tan, Y., Wang, X., Tian, C., Li, J., Fang, Y., Chen, Y., Cui, S., Zhang, G., 2020. Dual-modelling-based source apportionment of NOx in five Chinese megacities: providing the isotopic footprint from 2013 to 2014. Environ. Int. 137.

Zong, Z., Wang, X., Tian, C., Chen, Y., Fang, Y., Zhang, F., Li, C., Sun, J., Li, J., Zhang, G., 2017. First assessment of NOx sources at a regional background site in north China using isotopic analysis linked with modeling. Environ. Sci. Technol. 51, 5923–5931.